

Metal-Organic Framework Derived Electrocatalysts for Alkaline Oxygen Evolution Reaction

A thesis submitted towards the partial fulfilment of the
integrated BS-MS dual degree program

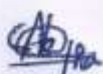


Submitted by
Aleena Jose
(Registration no.: **20181062**)

Under the guidance of
Prof. Ramanathan Vaidhyanathan
Department of Chemistry
Indian Institute of Science Education and Research, Pune

Certificate

This is to certify that the dissertation titled "**Metal-Organic Framework Derived Electrocatalysts for Alkaline Oxygen Evolution Reaction,**" submitted towards the partial fulfilment of the award of BS-MS dual degree at the Indian Institute of Science Education and Research (IISER), Pune, represents the work carried out by **Ms. Aleena Jose** (Roll No.- 20181062) at IISER, Pune, under the supervision of **Prof. Ramanathan Vaidhyanathan**, Professor, Department of Chemistry, and with the external expert **Dr. Subhadip Neogi**, Principal Scientist and Associate Professor, Central Salt and Marine Chemicals Research Institute (CSIR-CSMCRI), Bhavnagar.



Aleena Jose



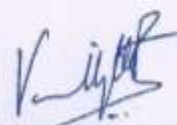
Prof. R. Vaidhyanathan

Declaration

I hereby declare that the matter embodied in the report entitled "**Metal-Organic Framework Derived Electrocatalysts for Alkaline Oxygen Evolution Reaction**" are the results of the work carried out by me at the Department of Chemistry, Indian Institute of Science Education and Research, Pune, under the supervision of Prof. R. Vaidhyanathan and the same has not been submitted elsewhere for any other degree.



Signature of Student



Signature of Supervisor

आर. वैद्यनाथन/R. Vaidhyanathan

प्रोफेसर / Professor

रसायनशास्त्र विभाग / Chemistry Department

भारतीय विज्ञान शिक्षा एवं अनुसंधान संस्थान

Indian Institute of Science Education & Research

पुणे / Pune- 411 008, भारत / India

Seal

Acknowledgement

I want to thank my thesis supervisor, Prof. R. Vaidhyanathan, for providing me with the opportunity to work on this project, for his constant guidance and encouragement. This project was an exciting research experience for me. I would also like to acknowledge my external expert, Dr. Subhadip Neogi from Central Salt and Marine Chemicals Research Institute (CSIR-CSMCRI), Bhavnagar, for reviewing my progress and providing valuable feedback during my mid-year presentation.

Many thanks to Himan Dev Singh, Deepak Rase, and Narugopal Manna, who mentored me during the various stages of my project and my present and former labmates Rinku Kushwaha, Chitvan Jain, Piyush Singh, Augustus Camillus, Liya S. Leo and Pragalbh Shekhar for their help and support in and out of the lab.

I am so grateful to have a fantastic bunch of friends who made my life at IISER cheerful and memorable.

Lastly but most importantly, my constant support system, my parents and my sisters, thank you for always being there for me and understanding me.

Table of contents

1. Introduction.....	1
1.1. Water splitting.....	1
1.1.1. Electrochemical water splitting.....	2
1.1.2. Alkaline OER electrocatalysis.....	3
1.2. Metal-organic frameworks (MOFs)	4
1.2.1. MOFs for gas separation and storage.....	5
1.2.2. MOFs in energy storage and conversion applications.....	5
1.3. MOFs as catalysts.....	5
1.4. MOF-based OER catalysts.....	5
1.4.1. Pristine MOFs as OER catalysts.....	5
1.4.2. MOF derived metal-free OER catalysts.....	6
1.4.3. MOF derived metal-based OER catalysts.....	6
1.5. Thesis overview.....	6
2. Materials and methods.....	8
2.1. Chemicals.....	8
2.2. Analytical characterization.....	8
2.2.1. Powder X-ray diffraction.....	8
2.3. Electrochemical characterization.....	8
2.3.1. Electrode preparation.....	8
2.3.2. Voltammetry studies.....	8
2.3.3. Chronoamperometry studies.....	9
2.4. Electrochemical calculations.....	9
2.4.1. Onset potential.....	9
2.4.2. Overpotential.....	9
2.4.3. Tafel slope.....	9
3. Synthesis and characterization.....	10
3.1. Synthesis.....	10
3.1.1. Synthesis of the MOFs.....	10
3.1.2. Post-synthesis pyrolysis of the MOFs.....	10
3.1.3. Synthesis of MOF composites.....	10
3.1.4. Synthesis of Ni _{0.8} Fe _{0.2} PyC.....	10

3.2. Characterization.....	11
3.2.1. Powder X-ray diffraction.....	11
3.2.2. FE-SEM & EDX.....	12
4. Results and discussion.....	13
4.1. Electrochemical studies.....	13
4.1.1. Voltammetry studies on pristine MOFs.....	13
4.1.2. Voltammetry studies on MOFs pyrolyzed at 300 °C.....	13
4.1.3. Voltammetry studies on MOFs pyrolyzed at 500 °C, 700 °C and 900 °C	14
4.1.4. Voltammetry studies on MOF composites.....	15
4.1.5. Voltammetry studies on NiPyC+FePyC composites.....	16
4.1.6. Voltammetry studies on Ni _{0.8} Fe _{0.2} PyC.....	18
4.2. Electrochemical characterizations.....	19
4.2.1. Tafel slope.....	19
4.2.2. Stability studies.....	19
5. Conclusion.....	21
6. Appendix.....	22
7. References.....	23

List of acronyms

1. μL	microlitre
2. 4-PyC	4 – Pyridine carboxylic acid or isonicotinic acid
3. ACN	Acetonitrile
4. atm	atmospheric pressure
5. AWE	Alkaline water electrolysis
6. CV	Cyclic voltammetry
7. DMF	Dimethylformamide
8. EDX	Energy dispersive X-ray analysis
9. EtOH	Ethanol
10. FE-SEM	Field emission scanning electron microscopy
11. HER	Hydrogen evolution reaction
12. LSV	Linear sweep voltammetry
13. mA/cm^2	milliampere per square centimetre
14. MJ/kg	Mega joule per kilogramme
15. mL	millilitre
16. MOF	Metal-organic framework
17. OER	Oxygen evolution reaction
18. PMWE	Proton membrane water electrolysis
19. PXRD	Powder X-ray diffraction
20. RHE	Reversible hydrogen electrode
21. THF	Tetrahydrofuran
22. η_{10}	Overpotential at 10 mA/cm^2

List of Figures

Fig. 1: Various types of water splitting

Fig. 2: Scheme showing water electrolysis with half-cell reactions of oxygen and hydrogen evolution reactions in acidic and alkaline conditions, along with the overall reactions.

Fig. 3: HER (left) and OER (right) polarisation plots indicating cathodic (left) and anodic (right) overpotentials, η_c and η_a , respectively.

Fig. 4: Mechanism of heterogeneously catalyzed OER in alkaline medium

Fig. 5: Applications of MOFs

Fig. 6: PXRD patterns of the pristine MOFs

Fig. 7: PXRD pattern of NiPyC+FePyC (8:2) composite and Ni_{0.8}Fe_{0.2}PyC

Fig. 8: FE-SEM morphology and EDX studies on Ni_{0.8}Fe_{0.2}PyC

Fig. 9: LSV curves of the as-made MOFs measured at a scan rate of 10 mV/s.

Fig. 10: The LSV curves of the samples made by pyrolyzing the four MOFs at 300 °C, 500 °C, 700 °C and 900 °C

Fig. 11: LSV curves of composites of

Fig. 12: The LSV curves of NiPyC+ FePyC composites mixed in various ratios

Fig. 13: LSV curves of Ni_{0.8}Fe_{0.2}PyC and the NiPyC+FePyC (8:2) composite.

Fig. 14: Tafel slope analysis of the NiPyC+FePyC composites mixed in different ratios.

Fig. 15: Stability studies of NiPyC+FePyC (8:2) using chronoamperometry plot over 12 hrs and CV curves recorded before and after chronoamperometry.

List of Tables

Table 1: The various synthesis conditions of the four isonicotinate MOFs

Table 2: The overpotential, η_{10} values, in mV, of the as-made MOFs and their pyrolyzed derivatives

Table 3: The overpotential, η_{10} values, in mV, of the composites of NiPyC with FePyC, CoPyC and MnPyC in the ratio 1:1 by weight

Table 4: Overpotential, η_{10} values, in mV, of NiPyC+FePyC composites mixed in various ratios.

Abstract

The challenge of the energy crisis and the demand for clean fuels is ever-growing. Hence, hydrogen is considered the future fuel because of its clean-burning properties. Electrochemically catalyzed splitting of water provides us with a carbon-free method for producing hydrogen and oxygen. Oxygen evolution reaction (OER) has a slow kinetics which affects the overall efficiency of the process of water splitting. To overcome the OER kinetics, ruthenium and iridium-based catalysts are used, but because of their low availability, high cost and unsatisfactory stability, they are non-economical for large-scale applications. Hence, active research is going on to develop catalysts based on cheaper transition metals for electrochemical OER. Recently, a variety of Metal-Organic Frameworks (MOFs) based OER electrocatalysts have emerged because of their highly porous nature and easy tunability of active sites. Through this work, nickel, cobalt, iron and manganese isonicotinate MOFs (Ni(4-PyC)₂, Co(4-PyC)₂, Fe(4-PyC)₂ and Mn(4-PyC)₂), and their derivatives have been synthesized, and their OER catalytic activity is studied. Electrochemical studies were done to assess the activity, kinetics and stability of these catalysts toward alkaline electrochemical OER.

1. Introduction

The global burden of the increasing energy demand to support the growing economy and population can no longer be put on conventional non-renewable sources, dominated by fossil fuels, as they are fast depleting and adversely affecting the environment by emitting greenhouse gases.¹ Hence, considerable efforts are motivated worldwide to develop sustainable and clean energy storage and conversion processes. Out of all the renewable energy sources, hydrogen stands out because of its high energy density (120 MJ/kg) and clean-burning properties. Today, hydrogen is produced on industrial scales using a plethora of catalysts and catalytic processes such as steam-reforming of natural gas, coal gasification, and steam-methane reformation, which are heavily dependent on fossil fuels.² On the other hand, water as a source of hydrogen possesses many advantages because of its ready availability, the high purity of the product obtained and the carbon neutrality of the whole process.

1.1 Water splitting

Water is split using an external energy source to produce hydrogen and oxygen. Depending on the external source, water splitting can be of various types, as summarised in **fig. 1**.^{3,4} Given its potential to solve the problem of intermittency of other renewable energy sources, electrochemical water splitting is gaining much attention these days.⁵

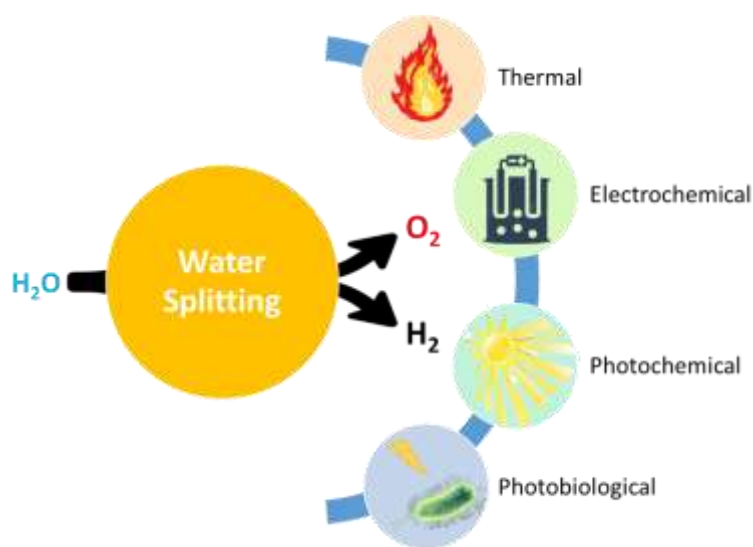


Fig. 1: Various types of water splitting

1.1.1 Electrochemical water splitting

The electrochemical splitting of water produces hydrogen and oxygen at the cathode and anode, respectively (**fig. 2a**). Catalysts play an important role in the electrochemical splitting of water because the kinetics of the oxygen evolution reaction (OER) happening at the anode is so slow that is affecting the overall process. An overpotential above the thermodynamic potential needs to be applied for these reactions to occur.¹ The conventional catalysts used for water splitting are based on ruthenium or iridium. But these catalysts are not suitable for large-scale electrolysis applications because of their high cost, poor availability and stability.⁶

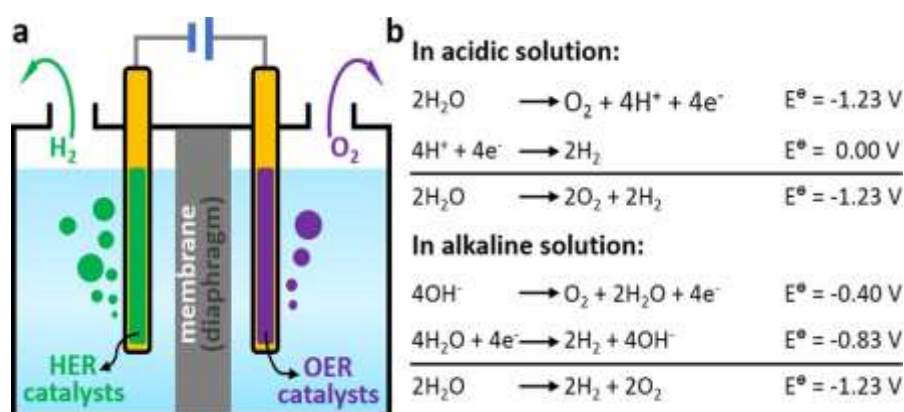


Fig. 2: a) Scheme showing water electrolysis with hydrogen evolving at the cathode and oxygen evolving at the anode b) half-cell reactions of oxygen and hydrogen evolution reactions in acidic and alkaline conditions along with the overall reactions. Reproduced from ref. 1.

Electrocatalytic water splitting uses extreme pH conditions so that the efficiency of the process is improved by providing the required H⁺ and OH⁻ ions, thus helping with the mass transport issues.^{1,2} Depending on the pH of the medium in which the electrolysis occurs, the mechanism and the active species are different. The half-cell reactions and their equilibrium half-cell potentials at standard conditions of 1 atm and 25 °C are shown in **fig. 2b**. The acidic pH low-temperature water electrolysis, known as Proton Membrane Water Electrolysis (PMWE), provides higher current densities but strictly requires noble-metal electrodes and a Nafion membrane which increases the overall cost. Hence, Alkaline Water Electrolysis (AWE) is more suitable for scaling up as non-noble metal electrodes can be used, and the membranes are cheaper.⁷ Active research is happening in this field to increase the efficiency of existing catalysts and to develop new catalysts based on cheaper transition metals with features like layered

and porous morphologies.² There are also reports of electrocatalysts with non-metallic active sites for water splitting.^{8,9}

The efficiency of the catalysts for electrochemical OER is measured using parameters like **1) Overpotential (η)**, which is the potential that has to be applied in addition to the thermodynamic potential to reach a particular current density value (**fig. 3**). Usually measured at 10 mA/cm² (η_{10}); **2) Tafel slope** gives a measure of the electron transfer kinetics of the catalysis. A low Tafel slope indicates that with a slight increase in the potential, large current densities are obtained;¹⁰ **3) Electrochemical stability** is measured to see if the proposed catalyst can provide constant current density at a constant applied potential for longer durations of time or vice versa; **4) Faradaic efficiency** compares the amount of O₂ obtained to the theoretical maximum possible, thus giving the efficiency of the catalysis. Finally, **5) Turn Over Frequency** gives the catalyst's efficiency by giving the amount of product formed per unit of catalyst per unit of time.

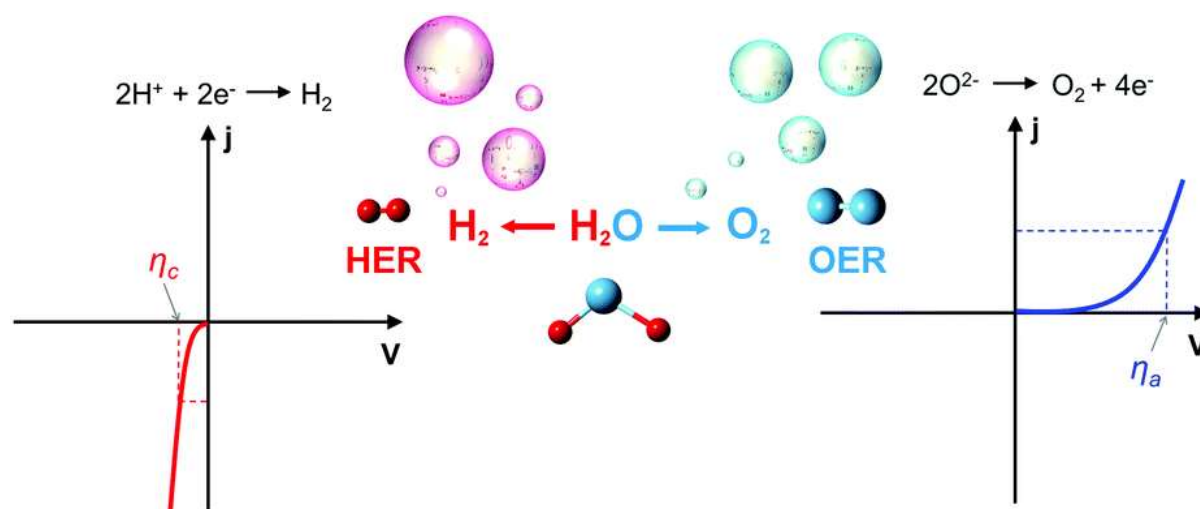


Fig. 3: HER (left) and OER (right) polarisation plots indicating cathodic (left) and anodic (right) overpotentials, η_c and η_a , respectively. Reproduced from ref. 10.

1.1.2 Alkaline OER Electrocatalysis

Oxygen evolution in water electrolysis happens in a multistep four electron-proton transfer mechanism making the kinetics challenging to catalyze. The plausible mechanism of OER electrocatalysis under alkaline conditions is shown in **fig. 4a**. There have been many studies recently to improve OER efficiency using catalysts.¹¹⁻

¹³ Nanoparticles of metals grown in porous frameworks were found to have low overpotentials.^{14,15}

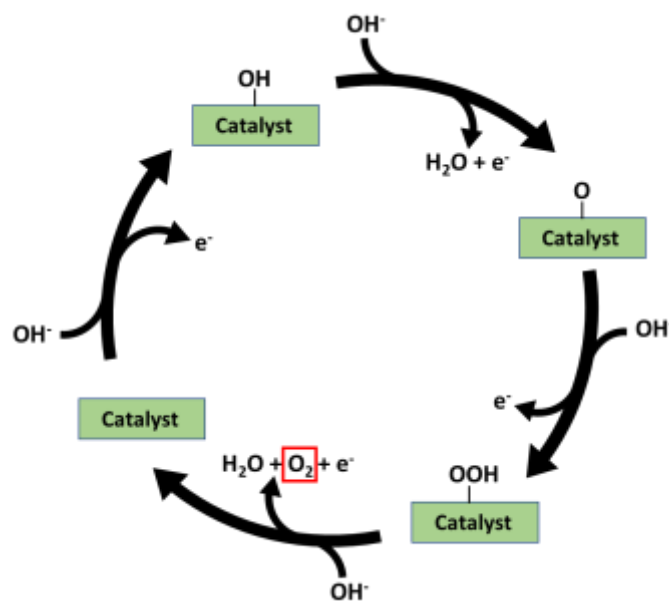


Fig. 4: Mechanism of heterogeneously catalyzed OER in alkaline medium

1.2 Metal-organic frameworks

Metal-organic frameworks (MOFs) are crystalline porous materials synthesized by coordinating metal ions to organic linker molecules. They are widely explored and have found applications in various fields, such as gas storage and separation,^{16–18} proton conduction,^{19,20} catalysis,²¹ etc., because of their easily tunable structure and high surface area (**Fig. 5**).

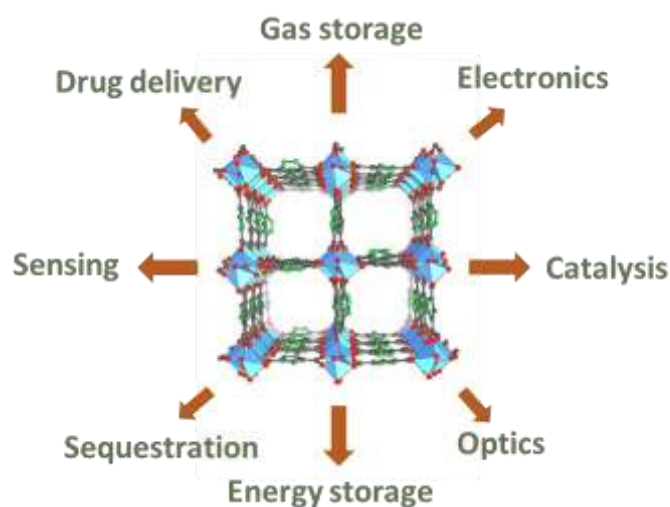


Fig. 5: Applications of MOFs²²

1.2.1 MOFs for gas separation and storage

MOFs have been studied for the storage of gases like hydrogen²³, methane²⁴ etc., to improve their ease of utilization as alternative fuels. MOFs have also found application in the separation and capture of gases like CO₂²⁵, a major greenhouse gas and Xe for nuclear fuel reprocessing and other applications.²⁶

1.2.2 MOFs in energy storage and conversion applications

The unique properties of MOFs find them good applications as proton and electron conduction materials.^{20,27} An example of MOF used in battery and supercapacitor applications is the Ni-MOF which shows high capacitance and exceptional stability.²⁸ Introduction of coordinating guest molecules like ethylene glycol and ions with a high degree of hydration like Cs⁺ into MOF frameworks have been observed to considerably lower the activation energy for proton conduction.^{20,29}

1.2.3 MOFs as catalysts

Catalysis with MOFs and their derivatives is an active research area because of their attractive features like high porosity, readily tuneable structure and high selectivity. UiO-66 is an example of a heterogeneous catalyst used in biomass conversion.³⁰ For the homogeneous catalysis of Suzuki coupling, MIL-101 has been used with encapsulated Pd ions.³¹

1.3 MOF-based OER catalysts

Various as-made MOFs and their modifications have been successfully studied for their OER electrocatalytic activity. The numerous uniformly distributed pore channels allowing the easy transport of reactants and evolution of the product gases, along with the homogeneous distribution of metal ions that serves as active sites, make MOFs excellent candidates as electrocatalysts for OER. Various types of MOF-based OER electrocatalysts are discussed in this section.

1.3.1 Pristine MOFs as OER catalysts

Catalysis with pristine MOFs is usually based on 2D nanosheets and/or bimetallic systems. The 2D morphology provides advantages like large surface area, easily accessible and exposed active sites and faster electron transfer.³² Incorporation of a second metal can modify the HOMO-LUMO levels, thus improving conductivity.

Thangasamy and coworkers reported NiCo 2D MOF grown on Ni foam requiring an overpotential of only 270 mV to give a current density of 50 mA/cm².³³

1.3.2 MOF derived metal-free OER catalysts

Carbon structures doped with heteroatom formed by the high-temperature pyrolysis of volatile metals like Zn-based MOFs are studied for their OER catalytic properties. Zhao's group reported a B-N dual doped porous carbon (BNPC) nanomaterials by the pyrolysis of MC-BIF-1S at 1100 °C under H₂ and Ar atmosphere. Thus synthesized BNPC was reported to have attained the current density of 10 mA/cm² at a potential of 1.55 V vs. RHE in a 6 M KOH solution.³⁴

1.3.3 MOF derived metal-based OER catalysts

Pyrolyzing MOFs is an effective route for synthesizing carbon-supported metal nanoparticles or metal derivatives for electrocatalysis applications. This approach also provides us with easy ways to introduce heteroatoms into the carbon framework, thus modifying the electronic structures and contributing to the overall conductivity of the materials. The temperature plays a critical role in the formation of conducting carbon. Nitrogen-doped graphene encapsulated Ni nanoparticles showing excellent HER and OER activity could be synthesized by the high-temperature pyrolysis of MOF-74 under inert conditions.³⁵

1.4 Thesis overview

This work studies the alkaline OER catalytic activity of four isonicotinate MOFs, namely, Ni(4-PyC)₂, Co(4-PyC)₂, Fe(4-PyC)₂ and Mn(4-PyC)₂ and their various modifications.^{25,36–38} The metals Ni, Co, Fe and Mn were chosen as they have been previously reported for their excellent electrocatalytic activity because of their good redox properties. Pyridinic nitrogen in the isonicotinate ligand is advantageous, as it plays a vital role in the OER catalytic behaviour.³⁹ Aromatic nitrogen tends to be incorporated more into the carbon skeleton after pyrolysis than aliphatic nitrogen.⁴⁰ Also, since two out of the six valencies of the metal ions are satisfied by the pyridinic N atoms of the isonicotinate linkers, there is a better chance of forming metal nitrides after pyrolysis. The OER catalytic activity of as-made MOFs was studied, followed by modifications via low-temperature and high-temperature pyrolysis. Low-temperature pyrolysis was done to create unsaturated coordination sites and defects in the framework that can form active sites and improve the conductivity of the MOFs,

respectively. The high-temperature pyrolysis under N_2 atmosphere to synthesize carbon-supported non-noble metal-based structures. Later, composites of the given MOFs were made by physically mixing them in different ratios and studied for their catalytic activity. The $Ni(4\text{-PyC})_2$ mixed with $Fe(4\text{-PyC})_2$ in the ratio 8:2 is observed to have good activity requiring an overpotential of only 280 mV to reach 10 mA/cm^2 geometric current density.

2. Materials and methods

2.1 Chemicals

All the chemical nickel acetate tetrahydrate, cobalt acetate tetrahydrate, isonicotinic acid and the solvents were all purchased from commercial sources and used without further purification.

2.2 Analytical characterization

2.2.1 Powder X-ray diffraction

The bulk purity and other structural characterizations of the samples were done using the powder XRDs using the Rigaku tabletop instrument and processed using PDXL software. Mercury software was used to calculate the simulated powder pattern from the single-crystal X-ray diffraction structures.

2.2.2 Field emission scanning electron microscopy

The FESEM images were obtained using an electron microscope with an integral charge compensator and embedded EsB and AsB detectors. The samples sonicated in THF were drop cast on silicon wafers and dried under vacuum.

2.3 Electrochemical characterization

2.3.1 Electrode preparation

5 mg of the sample was dispersed in 0.5 mL ethanol with 20 μL of 10% Nafion binder solution by sonicating for 1 hr. 100 μL of this solution was drop cast on a 1 cm^2 marked area of a toray paper in three turns and dried in a hot air oven. Thus, the catalyst loading is maintained at 1 mg/cm^2 .

2.3.2 Voltammetry studies

Voltammetry studies were carried out using AMETEK, and the data were analyzed using Versa Studio software. Three-electrode setup was used for the measurements with Hg/HgO electrode as the reference, Pt wire as the counter electrode, and the catalyst-coated toray paper as the working electrode. The electrolyte used was 1 M KOH solution, and the measurements were recorded at a scan rate of 10 mV/s in a potential window of 1 -1.7 V vs. Reversible Hydrogen Electrode (RHE).

The potential obtained in reference to Hg/HgO was converted to RHE by using the correction factor obtained by calibrating the Hg/HgO electrode (**fig. A1**). Hence for converting, the following formula was used.

$$\text{Potential vs. RHE (V)} = \text{Potential vs. Hg/HgO} + 0.917$$

The cyclic voltammogram of blank toray of 1 cm² area shows no activity (**fig. A2**). All the potentials mentioned in this thesis are in reference to RHE unless otherwise mentioned.

2.3.3 Chronoamperometry studies

Chronoamperometry studies were carried out using AMETEK, and the data were analyzed using Versa Studio software. The constant potential applied was 1.52 V, and the current was recorded for 12 hrs in the same static three-electrode setup.

2.4 Electrochemical calculations

2.4.1 Onset potential

The starting potential for the OER is called the onset potential for that catalyst. It is calculated as the potential required for the sample to reach a current density of 1 mA/cm² for OER.

2.4.2 Overpotential

The overpotential for OER catalysts is typically represented using the potential required to reach a geometric current density of 10 mA/cm². Thus, represented as η_{10} . It is calculated using the following formula;

$$\text{Overpotential } \eta_{10} = \text{Potential (V) required to reach } 10 \text{ mA/cm}^2 \text{ current density} - 1.23$$

2.4.3 Tafel slope

The Tafel slope is calculated as the slope of the straight line fitted on the plot of the log of current density in mA/cm² versus potential in volts vs. RHE.

The straight line fitted follows the equation;

$$\eta = a + b \log(j)$$

Where b , η and j denote the Tafel slope, overpotential and current density, respectively, and the y-intercept, a , gives the exchange current density.

3. Synthesis and characterization

3.1 Synthesis

3.1.1 Synthesis of MOFs

The MOFs were synthesized on a milligram scale via solvothermal synthesis. The metal salts were mixed with 2 mmol of isonicotinic acid or 4-pyridine carboxylic acid in various solvent combinations and were heated at 120 °C or 150 °C for 72 hrs to produce the four MOFs – Ni(4-PyC)₂, Co(4-PyC)₂, Fe(4-PyC)₂ and Mn(4-PyC)₂ referred to as NiPyC, CoPyC, FePyC and MnPyC respectively. **Table 1** summarises the synthesis procedure.^{25,36–38} After heating, the reaction mixtures were allowed to cool down slowly to room temperature over 12 hours. Crystals of all four MOFs could be observed under a microscope. The MOFs were extracted using vacuum filtration and were dried in a hot air oven.

Table 1: The various synthesis conditions of the four isonicotinate MOFs

MOF	Metal salt	Quantity	Solvent combination	Temperature
NiPyC	Nickel (II) acetate tetrahydrate	1 mmol (249 mg)	6 mL DMF + 4 mL ACN	150 °C
CoPyC	Cobalt (II) acetate tetrahydrate	1 mmol (249 mg)	5 mL DMF + 3 mL ACN	120 °C
FePyC	Iron (II) chloride tetrahydrate	1 mmol (199 mg)	2 mL DMF + 2 mL EtOH + 3 mL THF	120 °C
MnPyC	Manganese (II) acetate tetrahydrate	1 mmol (245 mg)	5 mL DMF + 3 mL ACN	120 °C

3.1.2 Post-synthesis pyrolysis of MOFs

The four MOFs were pyrolyzed in a tube furnace at different temperatures, specifically 300 °C, 500 °C, 700 °C and 900 °C, under the constant nitrogen flow (5 sccm).

3.1.3 Synthesis of MOF composites

The MOF composites were synthesized by physically mixing the two MOFs in the required ratio using a mortar and pestle.

3.1.4 Synthesis of Ni_{0.8}Fe_{0.2}PyC

Ni_{0.8}Fe_{0.2}PyC was synthesized solvothermally by mixing 0.8 mmol of nickel (II) acetate tetrahydrate and 0.2 mmol of iron (II) chloride tetrahydrate with 2 mmol of isonicotinic

acid in a 10 mL solution of DMF and ACN in 6:4 ratio. The mixture was made homogeneous, and triethyl amine (75 μ L) was added. The mixture was heated at 150 $^{\circ}$ C for 72 hours in an autoclave and cooled down slowly to room temperature. The samples were extracted using vacuum filtration and dried in a hot air oven.

3.2 Characterization

3.2.1 Powder X-ray Diffraction

The bulk purity of the MOFs was studied using powder x-ray diffraction by comparing the experimentally obtained PXRD pattern to the simulated powder pattern obtained using Mercury. PXRD patterns of the pyrolyzed samples are shown in **fig. 6**. The PXRD patterns of the NiPyC+FePyC (8:2) composite and the bimetallic Ni_{0.8}Fe_{0.2}PyC are shown in **fig. 7** along with the PXRD patterns of as-made NiPyC and FePyC. The composite shows the presence of both NiPyC as well as FePyC in its PXRD pattern, while that of Ni_{0.8}Fe_{0.2}PyC shows the characteristics of a MOF.

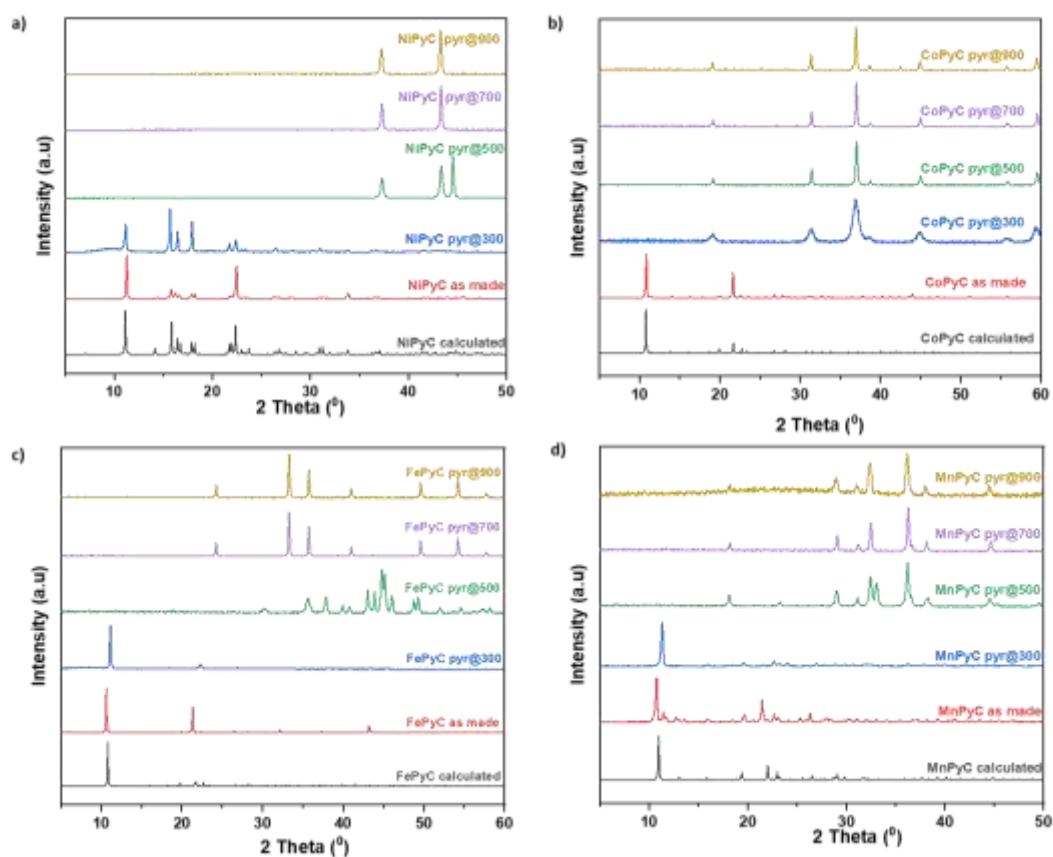


Fig. 6: PXRD patterns of the pristine MOFs a) NiPyC, b) CoPyC, c) FePyC and d) MnPyC; compared with the powder pattern calculated from their SCXRD structure and the PXRD pattern of the pyrolyzed samples.

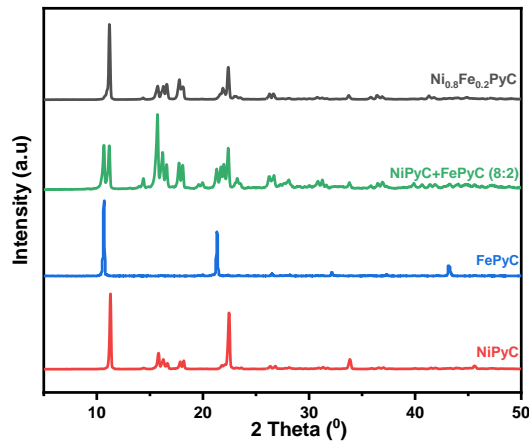


Fig. 7: PXR D pattern of NiPyC+FePyC (8:2) composite and Ni_{0.8}Fe_{0.2}PyC compared with that of NiPyC and FePyC, showing the presence of both MOFs in the former.

3.2.2 FE-SEM and EDX

To further characterize Ni_{0.8}Fe_{0.2}PyC, imaging and energy dispersive X-ray (EDX) analysis were performed using FE-SEM to study the morphology and the elemental composition. The morphology of Ni_{0.8}Fe_{0.2}PyC was found to be similar to that of NiPyC (**fig. 8a-c**), and from the EDX analysis, the presence of both nickel and iron in the ratio 8:2 could be verified (**fig. 8d,e**).

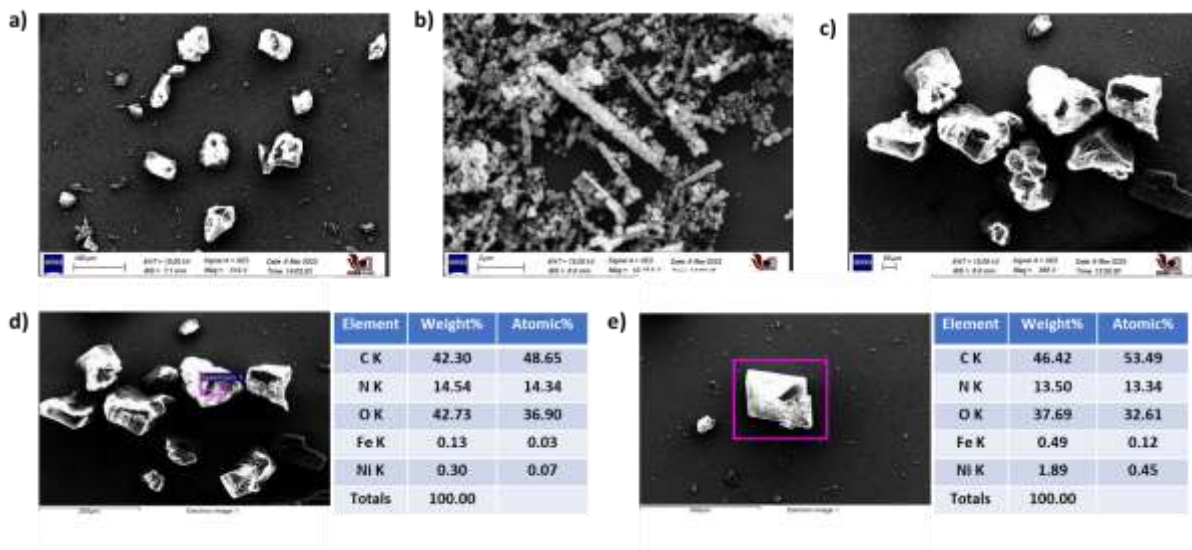


Fig. 8: FE-SEM morphology studies on a) NiPyC, b) FePyC, c) Ni_{0.8}Fe_{0.2}PyC and d,e) FE-SEM EDX studies of Ni_{0.8}Fe_{0.2}PyC showing the presence of Ni and Fe close to the ratio 8:2.

4. Results and discussions

4.1 Electrochemical studies

4.1.1 Voltammetry analysis on pristine MOFs

Initially, the OER catalytic activity of the pristine MOFs was studied in a three-electrode setup, as was explained in the materials and methods section, with 1 M KOH solution as the electrolyte. The linear sweep voltammograms of the pristine MOFs are shown in **fig. 9**. In the case of NiPyC, the oxidation peak of Ni^{2+} was overlapping with the current density from OER; hence the backward sweep of the voltammogram was used to calculate the overpotential (η_{10}) as is shown in the inset in **fig. 9**. The NiPyC shows the best overpotential of 377 mV at a current density of 10 mA/cm^2 . CoPyC showed an η_{10} of 412 mV. The FePyC and MnPyC MOFs showed poor activity and did not even reach the current density of 10 mA/cm^2 at 1.7 V to calculate their overpotential values.

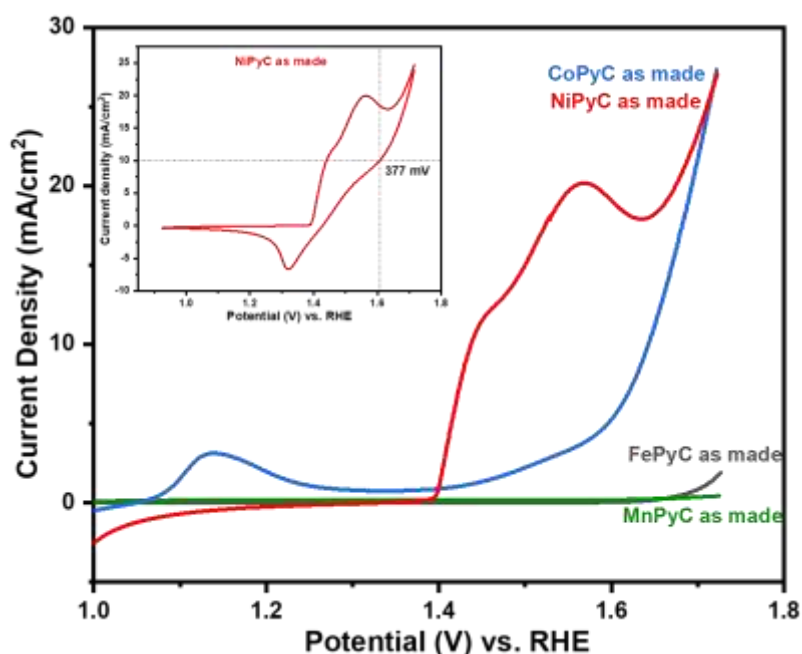


Fig. 9: LSV curves of the as-made MOFs measured at a scan rate of 10 mV/s. Inset showing CV curve of NiPyC and the calculation of η_{10} from the backward sweep.

4.1.2 Voltammetry studies on MOFs pyrolyzed at 300 °C

The MOFs were pyrolyzed at 300 °C for 8 hrs under the continuous flow of nitrogen so that it would create defects in their framework which can lower the HOMO-LUMO gap and thus increase the conductivity of the samples. The PXRDs of these samples are

shown in **fig. 6**. Except for CoPyC, the MOF structures were stable up to 300 °C. The samples were tested for OER catalytic activity in the same three-electrode set-up. The LSV curves of the samples are shown in **fig. 9a**. Only NiPyC showed a slight improvement in the activity, with the η_{10} decreasing from 377 mV in the case of as-made MOF to 360 mV when pyrolyzed at 300 °C for 8 hrs.

4.1.3 Voltammetry studies on MOFs pyrolyzed at 500 °C, 700 °C and 900 °C

To know the effects of calcination temperature on the structure and electrochemical performance, the MOFs were pyrolyzed at three different temperatures, 500 °C, 700 °C and 900 °C, for 8 hours under the continuous flow of nitrogen. By pyrolyzing the MOFs at high temperatures in the presence of nitrogen, the framework breaks down to form transition-metal-nitrogen moieties supported in carbon (M-N-Cs). The MOFs lost their crystalline framework on high-temperature pyrolysis, as evident from their PXRD patterns (**fig. 6**). The catalytic activity of the samples was tested in the three-electrode setup. As the LSV curves of the samples in **fig. 10b-d** show that the overpotential values increased, and the maximum current density reduced considerably after the high-temperature pyrolysis. The overpotential values of all the pyrolyzed samples are summarised in **table 2**.

Table 2: The overpotential, η_{10} values, in mV, of the as-made MOFs and their pyrolyzed derivatives

Pyrolysis temperature / MOFs	NiPyC	CoPyC	FePyC	MnPyC
As made	377	412	> 470	> 470
300 °C	360	> 470	> 470	> 470
500 °C	> 470	> 470	> 470	> 470
700 °C	> 470	> 470	> 470	> 470
900 °C	> 470	467	> 470	> 470

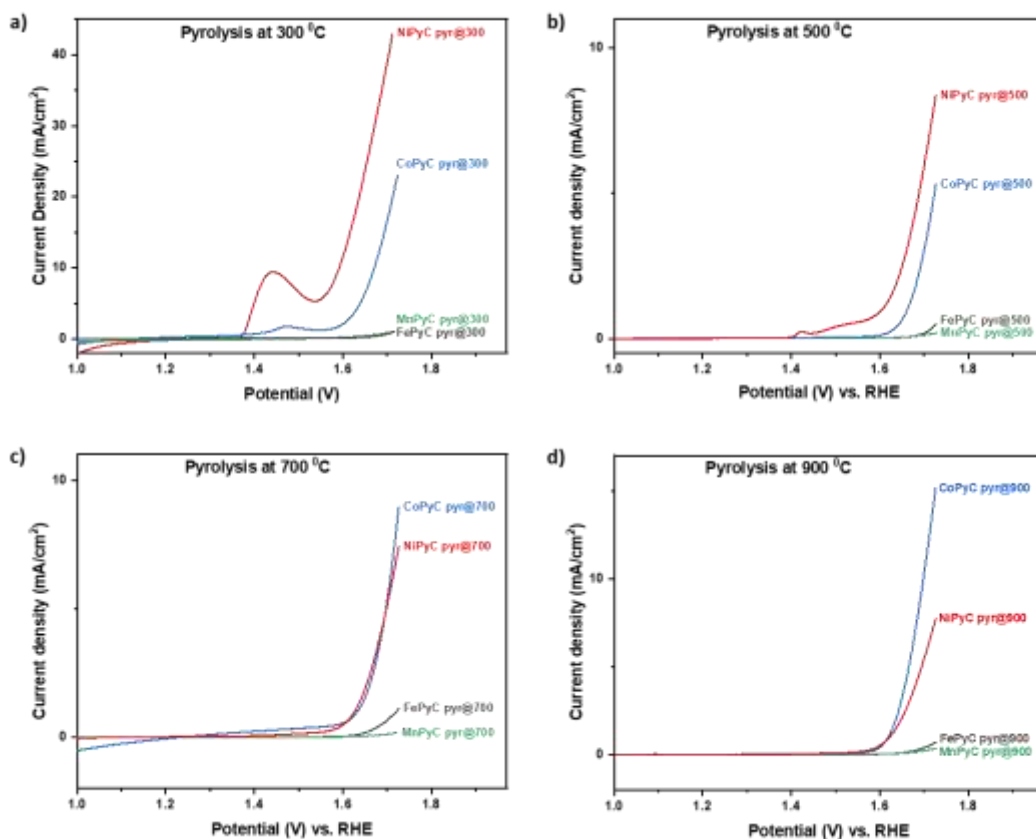


Fig. 10: The LSV curves of the samples made by pyrolyzing the four MOFs, NiPyC, CoPyC, FePyC and MnPyC, at four different temperatures, a) 300 °C, b) 500 °C, c) 700 °C and d) 900 °C

4.1.4 Voltammetry studies on MOF composites

NiPyC, so far, shows the best OER catalytic activity, and the crystalline framework is essential for the activity. Thus, to get the benefit of bimetallic active sites for the OER activity, we mixed NiPyC with the other three MOFs, i.e., MnPyC, CoPyC and FePyC in the ratio of 1:1 by weight using a mortar pestle.

The LSV curves of the composite catalysts were recorded in the three-electrode setup and are shown in **fig. 11**. The redox peak of NiPyC is considerably suppressed in the presence of FePyC. The oxidation peak from CoPyC starts around 1.15 V vs. RHE and overlaps with that of NiPyC, leading to the OER to begin only at around 1.5 V in the case of NiPyC, CoPyC mixture. MnPyC does not seem to affect the redox behaviour of NiPyC in any way, and it starts around 1.3 V. Still, the catalytic activity is relatively low, solely contributed by the 0.5 mg NiPyC in the sample leading to the least

overall current density. We calculated the η_{10} values for the three combinations from the LSV curves (**table 3**). The NiPyC+FePyC gave the least η_{10} of 304 mV.

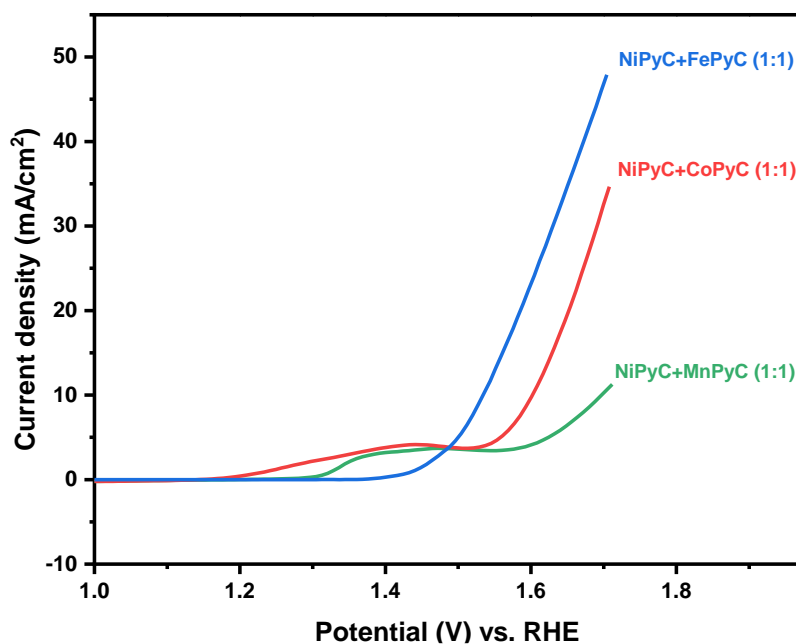


Fig. 11: LSV curves of composites of NiPyC with the other three MOFs, MnPyC, CoPyC and FePyC, in the ratio 1:1 by weight (NiPyC+MnPyC (1:1), NiPyC+CoPyC (1:1) and NiPyC+FePyC (1:1)) recorded at a scan rate of 10 mV/s.

Table 3: The overpotential, η_{10} values, in mV, of the composites of NiPyC with FePyC, CoPyC and MnPyC in the ratio 1:1 by weight.

Sample	Overpotential, η_{10}
NiPyC+FePyC (1:1)	304
NiPyC+CoPyC (1:1)	372
NiPyC+MnPyC (1:1)	465

4.1.5 Voltammetry studies on NiPyC+FePyC composites

The NiPyC, FePyC mixed composite shows improved OER catalytic activity. Hence, we mixed NiPyC and FePyC in various ratios, such as (8:2), (6:4), (5:5), (4:6) and (2:8). Comparing the LSV curves of the five combinations (**fig. 12**), the maximum current attained at 1.7 V vs. RHE decreases as the amount of FePyC increases in the mixture. The η_{10} follows the opposite trend and is summarised in **table 4**.

NiPyC+FePyC (8:2) shows the highest current density of 65 mA/cm² at a potential of 1.7 V. The oxidation peak of NiPyC overlaps with the OER; hence we calculated the η_{10} for this sample from its backward sweep like in the case of NiPyC as-made sample (inset in **fig.12**). It turns out that NiPyC, when physically mixed with FePyC in the ratio 8:2 by weight, requires an overpotential of only 280 mV for the current density from OER to reach 10 mA/cm². The onset potential for OER using this mixture was 1.46 V vs. RHE. The PXRD of this composite in **fig. 7** clearly shows the presence of both NiPyC and FePyC MOFs in it. To see if lowering the FePyC:NiPyC ratio will further reduce the overpotential, we mixed NiPyC and FePyC in the ratio 9:1 by weight and studied its catalytic activity. It could be seen from **fig. 12** that for NiPyC+FePyC (9:1), the maximum current lowered, and the η_{10} increased. This could be because the FePyC in 1:9 ratio is insufficient for suppressing the redox of the NiPyC and hence increasing the overpotential.

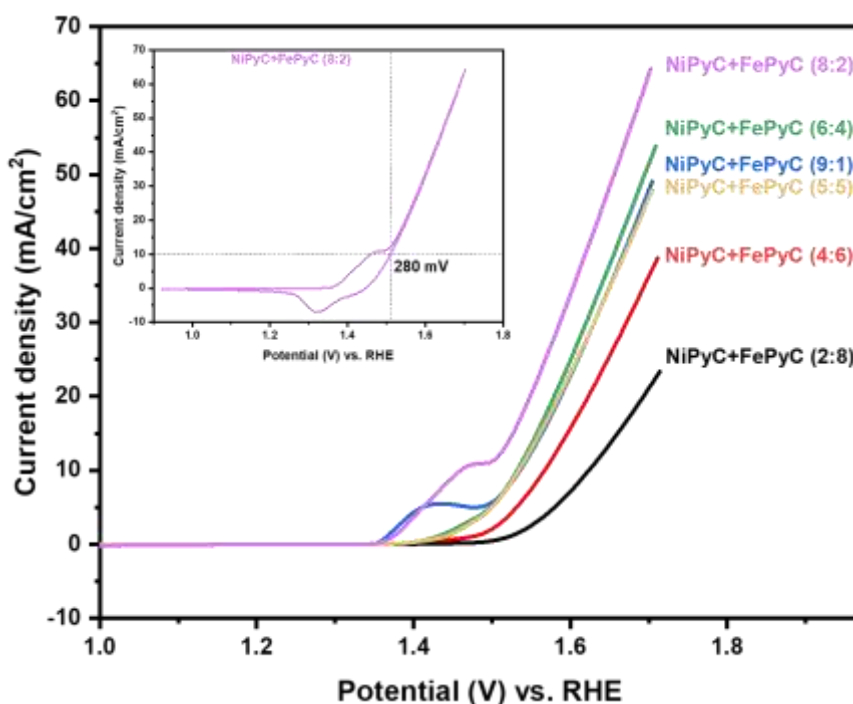


Fig. 12: The LSV curves of NiPyC+ FePyC composites mixed in various ratios by weight. Inset showing the CV curve of NiPyC+FePyC (8:2) sample and the calculation of η_{10} for the sample from the backward sweep of the voltammogram.

Table 4: Overpotential, η_{10} values, in mV, of NiPyC+FePyC composites mixed in various ratios.

NiPyC	FePyC	Overpotential, η_{10}
10	0	377
9	1	303
8	2	280
6	4	301
5	5	304
4	6	337
2	8	392
0	10	> 470

4.1.6 Voltammetry studies on Ni_{0.8}Fe_{0.2}PyC

Since the NiPyC+FePyC (8:2) composite gave us the least overpotential, we tried to synthesize Ni_{0.8}Fe_{0.2}PyC MOF under the synthesis conditions of NiPyC, solvothermally and characterized using PXRD, FE-SEM and EDX (fig. 7,8). The sample was tested for OER catalytic activity in the three-electrode setup. The η_{10} was calculated from the LSV from fig. 13 and was found to be 286 mV. This is almost the same as that of the physical mixture of the two MOFs, showing no improvement in the OER activity. This could mean that the presence of FePyC in the vicinity Ni active site is enough to boost the catalyst activity, but more studies are needed to verify this.

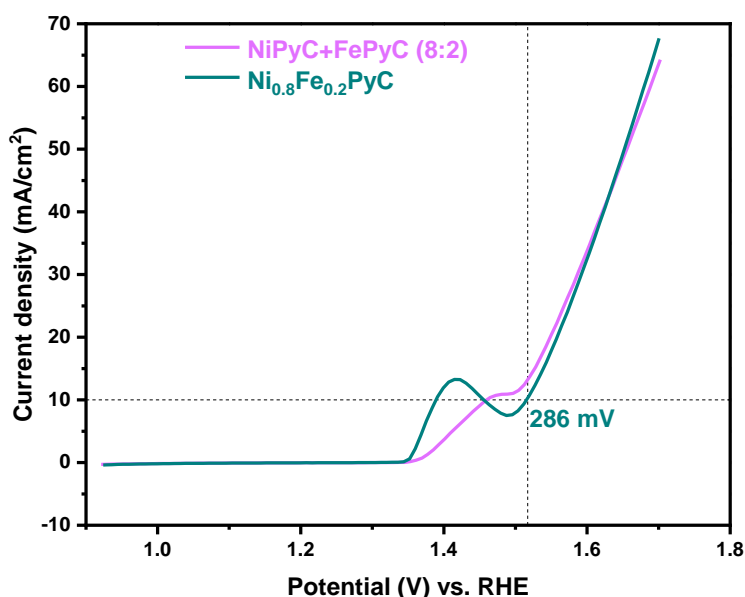


Fig. 13: LSV curves of the solvothermally synthesized Ni_{0.8}Fe_{0.2}PyC and the NiPyC+FePyC (8:2) composite.

4.2 Electrochemical characterizations

4.2.1 Tafel slope

To compare the kinetics of the four combinations of NiPyC+FePyC composites, the \log_{10} of the corresponding current density in mA/cm^2 versus the potential in volts in reference to RHE starting from the onset potential was plotted. The slope of the straight line fitted to this plot gave us the Tafel slope. The Tafel slopes for the various NiPyC+FePyC composites are shown in **fig. 14**. Of all the samples, the NiPyC+FePyC composite mixed in the ratio 8:2 was found to have the lowest Tafel slope of 95 mV dec^{-1} . The low Tafel slope for the NiPyC+FePyC(8:2) catalyst signifies the better OER kinetics of the sample.

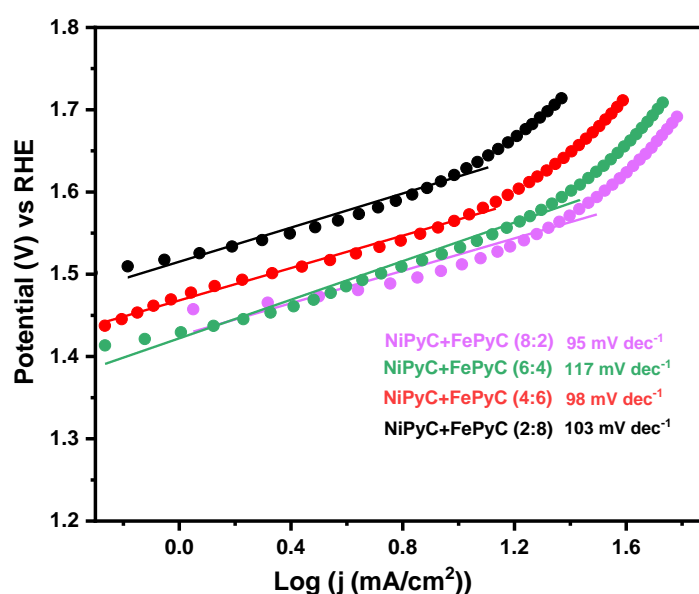


Fig. 14: Tafel slope analysis of the NiPyC+FePyC composites mixed in different weight ratios.

4.2.2 Stability studies

The electrochemical stability of the best performing NiPyC+FePyC (8:2) was studied by performing chronoamperometry analysis in a static setup at an applied potential of 1.52 mV vs. RHE for 12 hrs. The current density decreased with time, with 60% retention after 12 hours (**fig. 15a**). This drop in the current density is probably because the oxygen bubbles formed collected over the surface of the catalyst blocking the entry of OH^- ions into the active sites.

To verify this, after the chronoamperometry measurements we took the working electrode out of the electrolyte for a brief amount of time, connected it back in the

circuit and ran another set of cyclic voltammograms. This was done to remove any oxygen bubbles collected over the catalyst surface. A comparative plot of the initial CV cycle and one recorded after chronoamperometry is shown in **fig. 15b**. There is only a difference of 15 mV in the overpotential and a 12 mA/cm² drop in the maximum current density attained at 1.7 V vs. RHE. This shows that the catalyst is reasonably stable.

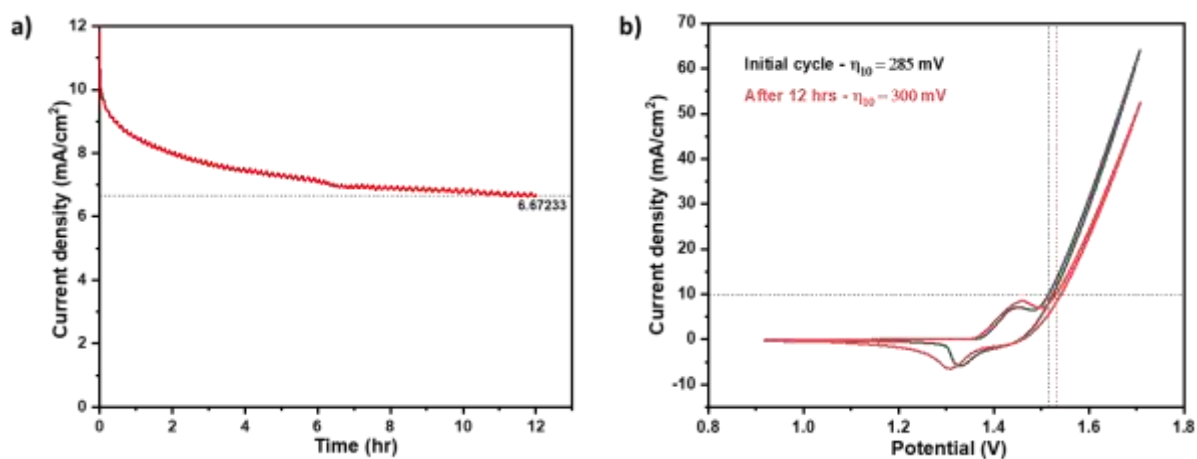


Fig. 15: a) Chronoamperometry plot showing 60% retention in current density over 12 hrs at an applied potential of 1.52 mV; b) CV curves recorded before and after chronoamperometry measurement for the NiPyC+FePyC (8:2) sample.

5. Conclusion

There are several reports on Fe improving the OER activity of Ni-based catalysts.^{41,42} In this work, we studied the alkaline OER catalytic activity of Ni, Co, Fe and Mn isonicotinate MOFs, their pyrolyzed modifications and composites, especially the NiPyC+FePyC composite. The addition of FePyC considerably reduced the redox of Ni²⁺/Ni³⁺ and other higher oxidation states in the NiPyC sample and improved the catalytic activity of the samples. We have found that of all the composites NiPyC mixed with FePyC in the ratio 8:2, by weight, shows the lowest overpotential of 280 mV to reach the current density of 10 mA/cm². The sample also shows a Tafel slope of 95 mV dec⁻¹ indicating kinetic performance. The chronoamperometry measurement showed reasonably good stability for the proposed catalyst, and this could also be verified from the CV recorded after 12 hours of chronoamperometry.

6. Appendix

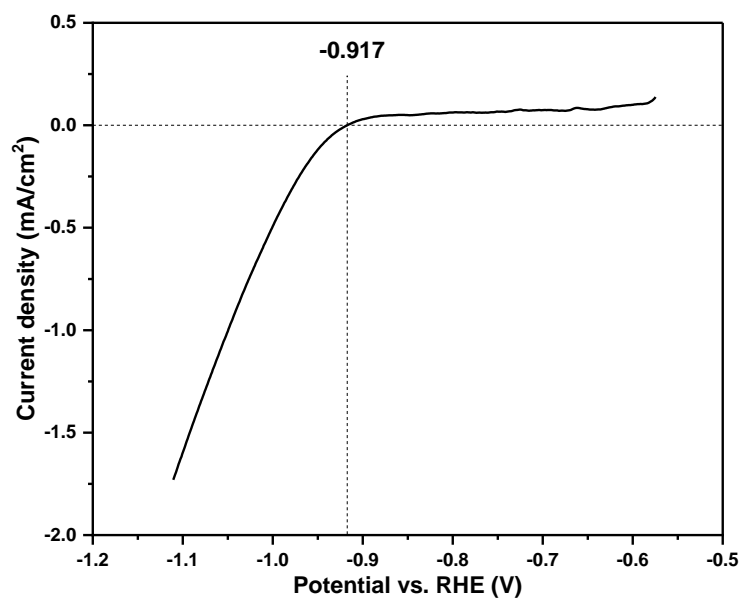


Fig. A1: Calibration plot of Hg/HgO vs. RHE showing the correction factor of -0.917 V.

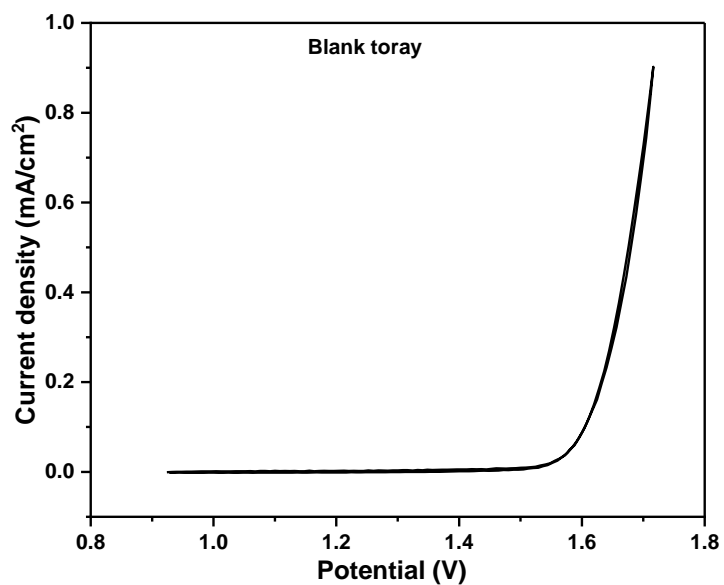


Fig. A2: CV plot of blank toray paper showing no redox or OER activities.

7. References

- (1) You, B.; Sun, Y. Innovative Strategies for Electrocatalytic Water Splitting. *Accounts of Chemical Research* **2018**. <https://doi.org/10.1021/acs.accounts.8b00002>.
- (2) Xiao, X.; Yang, L.; Sun, W.; Chen, Y.; Yu, H.; Li, K.; Jia, B.; Zhang, L.; Ma, T. Electrocatalytic Water Splitting: From Harsh and Mild Conditions to Natural Seawater. *Small* **2022**, *18* (11), 2105830. <https://doi.org/10.1002/sml.202105830>.
- (3) Vaidhyanathan, R. Covalent Organic Frameworks as Tunable Supports for HER, OER, and ORR Catalysts: A New Addition to Heterogeneous Electrocatalysts. *Molecular Architectonics and Nanoarchitectonics* **2022**, 389–444. https://doi.org/10.1007/978-981-16-4189-3_16.
- (4) Tahir, M. B.; Batool, A. Recent Development in Sustainable Technologies for Clean Hydrogen Evolution: Current Scenario and Future Perspectives. In *Sustainable Materials and Green Processing for Energy Conversion*; Elsevier, 2022; pp 97–130. <https://doi.org/10.1016/B978-0-12-822838-8.00008-9>.
- (5) Wang, S.; Lu, A.; Zhong, C.-J. Hydrogen Production from Water Electrolysis: Role of Catalysts. *Nano Convergence* **2021**, *8* (1), 1–23. <https://doi.org/10.1186/s40580-021-00254-x>.
- (6) Suryanto, B. H. R.; Wang, Y.; Hocking, R. K.; Adamson, W.; Zhao, C. Overall Electrochemical Splitting of Water at the Heterogeneous Interface of Nickel and Iron Oxide. *Nat Commun* **2019**, *10* (1), 1–10. <https://doi.org/10.1038/s41467-019-13415-8>.
- (7) Kou, T.; Wang, S.; Li, Y. Perspective on High-Rate Alkaline Water Splitting. *ACS Materials Letters* **2021**. <https://doi.org/10.1021/acsmaterialslett.0c00536>.
- (8) Xu, Y.; Kraft, M.; Xu, R. Metal-Free Carbonaceous Electrocatalysts and Photocatalysts for Water Splitting. *Chem. Soc. Rev.* **2016**, *45* (11), 3039–3052. <https://doi.org/10.1039/C5CS00729A>.
- (9) J, Z.; Z, Z.; X, X.; L, D. A Metal-Free Bifunctional Electrocatalyst for Oxygen Reduction and Oxygen Evolution Reactions. *Nature nanotechnology* **2015**, *10* (5). <https://doi.org/10.1038/nnano.2015.48>.
- (10) Suen, N.-T.; Hung, S.-F.; Quan, Q.; Zhang, N.; Xu, Y.-J.; Chen, H. M. Electrocatalysis for the Oxygen Evolution Reaction: Recent Development and Future Perspectives. *Chem. Soc. Rev.* **2017**, *46* (2), 337–365. <https://doi.org/10.1039/C6CS00328A>.
- (11) Shi, Y.; Zhang, D.; Miao, H.; Zhan, T.; Lai, J. Design of NiFe-Based Nanostructures for Efficient Oxygen Evolution Electrocatalysis. *Electrochemical Science Advances* **2022**, *2* (2), e2100052. <https://doi.org/10.1002/elsa.202100052>.
- (12) Bezerra, L. S.; Maia, G. Developing Efficient Catalysts for the OER and ORR Using a Combination of Co, Ni, and Pt Oxides along with Graphene Nanoribbons and NiCo₂O₄. *J. Mater. Chem. A* **2020**, *8* (34), 17691–17705. <https://doi.org/10.1039/D0TA05908K>.
- (13) Duan, Y.; Huang, Z.; Ren, J.; Dong, X.; Wu, Q.; Jia, R.; Xu, X.; Shi, S.; Han, S. Highly Efficient OER Catalyst Enabled by in Situ Generated Manganese Spinel on Polyaniline with Strong Coordination. *Dalton Trans.* **2022**, *51* (23), 9116–9126. <https://doi.org/10.1039/D2DT01236G>.
- (14) Mullangi, D.; Dhavale, V.; Shalini, S.; Nandi, S.; Collins, S.; Woo, T.; Kurungot, S.; Vaidhyanathan, R. Low-Overpotential Electrocatalytic Water Splitting with Noble-Metal-Free Nanoparticles Supported in a Sp³ N-Rich Flexible COF. *Advanced Energy Materials* **2016**, *6* (13), 1600110. <https://doi.org/10.1002/aenm.201600110>.
- (15) Nandi, S.; Singh, S. K.; Mullangi, D.; Illathvalappil, R.; George, L.; Vinod, C. P.; Kurungot, S.; Vaidhyanathan, R. Low Band Gap Benzimidazole COF Supported Ni₃N as Highly Active OER Catalyst. *Advanced Energy Materials* **2016**, *6* (24), 1601189. <https://doi.org/10.1002/aenm.201601189>.
- (16) Nandi, S.; De Luna, P.; Daff, T. D.; Rother, J.; Liu, M.; Buchanan, W.; Hawari, A. I.; Woo, T. K.; Vaidhyanathan, R. A Single-Ligand Ultra-Microporous MOF for Precombustion CO₂ Capture and Hydrogen Purification. *Science Advances* **2015**, *1* (11), e1500421. <https://doi.org/10.1126/sciadv.1500421>.

- (17) Lin, J.-B.; Nguyen, T. T. T.; Vaidhyanathan, R.; Burner, J.; Taylor, J. M.; Durekova, H.; Akhtar, F.; Mah, R. K.; Ghaffari-Nik, O.; Marx, S.; Fylstra, N.; Iremonger, S. S.; Dawson, K. W.; Sarkar, P.; Hovington, P.; Rajendran, A.; Woo, T. K.; Shimizu, G. K. H. A Scalable Metal-Organic Framework as a Durable Physisorbent for Carbon Dioxide Capture. *Science* **2021**, *374* (6574), 1464–1469. <https://doi.org/10.1126/science.abi7281>.
- (18) Nandi, S.; Singh, H. D.; Chakraborty, D.; Maity, R.; Vaidhyanathan, R. Deciphering the Weak CO₂···Framework Interactions in Microporous MOFs Functionalized with Strong Adsorption Sites—A Ubiquitous Observation. *ACS Appl. Mater. Interfaces* **2021**, *13* (21), 24976–24983. <https://doi.org/10.1021/acsami.1c05845>.
- (19) Hurd, J. A.; Vaidhyanathan, R.; Thangadurai, V.; Ratcliffe, C. I.; Moudrakovski, I. L.; Shimizu, G. K. H. Anhydrous Proton Conduction at 150 °C in a Crystalline Metal–Organic Framework. *Nature Chem* **2009**, *1* (9), 705–710. <https://doi.org/10.1038/nchem.402>.
- (20) Shalini, S.; Dhavale, V. M.; Eldho, K. M.; Kurungot, S.; Ajithkumar, T. G.; Vaidhyanathan, R. 1000-Fold Enhancement in Proton Conductivity of a MOF Using Post-Synthetically Anchored Proton Transporters. *Sci Rep* **2016**, *6* (1), 1–8. <https://doi.org/10.1038/srep32489>.
- (21) Karve, V. V.; Vieira, A. N.; Stoian, D.; Trukhina, O.; Queen, W. L. Solid-State Synthesis of a MOF/Polymer Composite for Hydrodeoxygenation of Vanillin. *Chem. Commun.* **2022**, *58* (82), 11559–11562. <https://doi.org/10.1039/D2CC03110H>.
- (22) Fathieh, F.; Kalmutzki, M. J.; Kapustin, E. A.; Waller, P. J.; Yang, J.; Yaghi, O. M. Practical Water Production from Desert Air. *Science Advances* **2018**, *4* (6), eaat3198. <https://doi.org/10.1126/sciadv.aat3198>.
- (23) Xu, J.; Liu, J.; Li, Z.; Wang, X.; Xu, Y.; Chen, S.; Wang, Z. Optimized Synthesis of Zr(IV) Metal Organic Frameworks (MOFs-808) for Efficient Hydrogen Storage. *New J. Chem.* **2019**, *43* (10), 4092–4099. <https://doi.org/10.1039/C8NJ06362A>.
- (24) Peng, Y.; Krungleviciute, V.; Eryazici, I.; Hupp, J. T.; Farha, O. K.; Yildirim, T. Methane Storage in Metal–Organic Frameworks: Current Records, Surprise Findings, and Challenges. *J. Am. Chem. Soc.* **2013**, *135* (32), 11887–11894. <https://doi.org/10.1021/ja4045289>.
- (25) Singh, H. D.; Nandi, S.; Chakraborty, D.; Singh, K.; Vinod, C. P.; Vaidhyanathan, R. Coordination Flexibility Aided CO₂-Specific Gating in an Iron Isonicotinate MOF. *Chemistry – An Asian Journal* **2022**, *17* (4), e202101305. <https://doi.org/10.1002/asia.202101305>.
- (26) Chakraborty, D.; Nandi, S.; Maity, R.; Motkuri, R. K.; Han, K. S.; Collins, S.; Humble, P.; Hayes, J. C.; Woo, T. K.; Vaidhyanathan, R.; Thallapally, P. K. An Ultra-Microporous Metal–Organic Framework with Exceptional Xe Capacity. *Chemistry – A European Journal* **2020**, *26* (55), 12544–12548. <https://doi.org/10.1002/chem.202002331>.
- (27) Su, J.; He, W.; Li, X.-M.; Sun, L.; Wang, H.-Y.; Lan, Y.-Q.; Ding, M.; Zuo, J.-L. High Electrical Conductivity in a 2D MOF with Intrinsic Superprotonic Conduction and Interfacial Pseudo-Capacitance. *Matter* **2020**, *2* (3), 711–722. <https://doi.org/10.1016/j.matt.2019.12.018>.
- (28) Yang, C.; Li, X.; Yu, L.; Liu, X.; Yang, J.; Wei, M. A New Promising Ni-MOF Superstructure for High-Performance Supercapacitors. *Chem. Commun.* **2020**, *56* (12), 1803–1806. <https://doi.org/10.1039/C9CC09302H>.
- (29) Shalini, S.; Aggarwal, S.; Singh, S. K.; Dutt, M.; Ajithkumar, T. G.; Vaidhyanathan, R. 10000-Fold Enhancement in Proton Conduction by Doping of Cesium Ions in a Proton-Conducting Zwitterionic Metal–Organic Framework. *European Journal of Inorganic Chemistry* **2016**, *2016* (27), 4382–4386. <https://doi.org/10.1002/ejic.201600364>.
- (30) Ponchai, P.; Adpakpang, K.; Thongratkaew, S.; Chaipojjana, K.; Wannapaiboon, S.; Siwaipram, S.; Faungnawakij, K.; Bureekaew, S. Engineering Zirconium-Based UiO-66 for Effective Chemical Conversion of D-Xylose to Lactic Acid in Aqueous Condition. *Chem. Commun.* **2020**, *56* (58), 8019–8022. <https://doi.org/10.1039/D0CC03424J>.
- (31) Li, J.-X.; Li, X.; Tang, H.; Zhang, Y.-Y.; Han, Z.-B. Palladium Nanoparticles Encapsulated in MIL-101-NH₂ Catalyzed One-Pot Reaction of Suzuki-Knoevenagel

- Reaction. *Inorganic Chemistry Communications* **2019**, *103*, 82–86. <https://doi.org/10.1016/j.inoche.2019.02.042>.
- (32) Li, S.; Gao, Y.; Li, N.; Ge, L.; Bu, X.; Feng, P. Transition Metal-Based Bimetallic MOFs and MOF-Derived Catalysts for Electrochemical Oxygen Evolution Reaction. *Energy Environ. Sci.* **2021**, *14* (4), 1897–1927. <https://doi.org/10.1039/D0EE03697H>.
- (33) Thangasamy, P.; Shanmuganathan, S.; Subramanian, V. A NiCo-MOF Nanosheet Array Based Electrocatalyst for the Oxygen Evolution Reaction. *Nanoscale Adv.* **2020**, *2* (5), 2073–2079. <https://doi.org/10.1039/D0NA00112K>.
- (34) Qian, Y.; Hu, Z.; Ge, X.; Yang, S.; Peng, Y.; Kang, Z.; Liu, Z.; Lee, J. Y.; Zhao, D. A Metal-Free ORR/OER Bifunctional Electrocatalyst Derived from Metal-Organic Frameworks for Rechargeable Zn-Air Batteries. *Carbon* **2017**, *111*, 641–650. <https://doi.org/10.1016/j.carbon.2016.10.046>.
- (35) Y, X.; W, T.; B, Z.; S, Y.; Y, H.; M, K.; R, X. Nickel Nanoparticles Encapsulated in Few-Layer Nitrogen-Doped Graphene Derived from Metal-Organic Frameworks as Efficient Bifunctional Electrocatalysts for Overall Water Splitting. *Advanced materials (Deerfield Beach, Fla.)* **2017**, *29* (11). <https://doi.org/10.1002/adma.201605957>.
- (36) Nandi, S.; Collins, S.; Chakraborty, D.; Banerjee, D.; Thallapally, P. K.; Woo, T. K.; Vaidyanathan, R. *Ultralow Parasitic Energy for Postcombustion CO₂ Capture Realized in a Nickel Isonicotinate Metal–Organic Framework with Excellent Moisture Stability*. ACS Publications. <https://doi.org/10.1021/jacs.6b10455>.
- (37) Nandi, S.; Luna, P. D.; Maity, R.; Chakraborty, D.; Daff, T.; Burns, T.; Woo, T. K.; Vaidyanathan, R. Imparting Gas Selective and Pressure Dependent Porosity into a Non-Porous Solid via Coordination Flexibility. *Mater. Horiz.* **2019**, *6* (9), 1883–1891. <https://doi.org/10.1039/C9MH00133F>.
- (38) *New metal–organic frameworks derived from pyridine-3,5-dicarboxylic acid: structural diversity arising from the addition of templates into the reaction systems - CrystEngComm (RSC Publishing)*. <https://pubs.rsc.org/en/content/articlelanding/2020/CE/C9CE02006C> (accessed 2023-04-10).
- (39) Lei, Y.; Wei, L.; Zhai, S.; Wang, Y.; Enis Karahan, H.; Chen, X.; Zhou, Z.; Wang, C.; Sui, X.; Chen, Y. Metal-Free Bifunctional Carbon Electrocatalysts Derived from Zeolitic Imidazolate Frameworks for Efficient Water Splitting. *Materials Chemistry Frontiers* **2018**, *2* (1), 102–111. <https://doi.org/10.1039/C7QM00452D>.
- (40) Wang, X.; Zhou, J.; Fu, H.; Li, W.; Fan, X.; Xin, G.; Zheng, J.; Li, X. MOF Derived Catalysts for Electrochemical Oxygen Reduction. *J. Mater. Chem. A* **2014**, *2* (34), 14064–14070. <https://doi.org/10.1039/C4TA01506A>.
- (41) Wang, J.; Gan, L.; Zhang, W.; Peng, Y.; Yu, H.; Yan, Q.; Xia, X.; Wang, X. In Situ Formation of Molecular Ni-Fe Active Sites on Heteroatom-Doped Graphene as a Heterogeneous Electrocatalyst toward Oxygen Evolution. *Science Advances* **2018**, *4* (3), eaap7970. <https://doi.org/10.1126/sciadv.aap7970>.
- (42) Görlin, M.; Ferreira de Araújo, J.; Schmies, H.; Bernsmeier, D.; Dresch, S.; Glied, M.; Jusys, Z.; Cherev, P.; Kraehnert, R.; Dau, H.; Strasser, P. Tracking Catalyst Redox States and Reaction Dynamics in Ni–Fe Oxyhydroxide Oxygen Evolution Reaction Electrocatalysts: The Role of Catalyst Support and Electrolyte pH. *J. Am. Chem. Soc.* **2017**, *139* (5), 2070–2082. <https://doi.org/10.1021/jacs.6b12250>.